INTERNATIONAL SOCIETY
FOR ROCK MECHANICS

SOCIETE INTERNATIONALE
DE MECANIQUE DES ROCHES

INTERNATIONALE GESELLSCHAFT
FÜR FELSMECHANIK

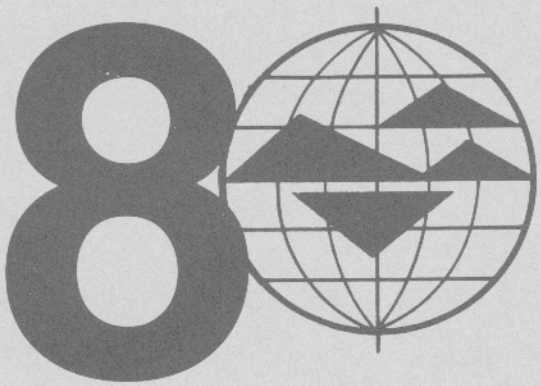

International Congress on
Rock Mechanics

Congrès International
de Mécanique des Roches

Internationaler Kongress
über Felsmechanik

# PROCEEDINGS / COMPTES-RENDUS / BERICHTE

Editor / Editeur / Herausgeber
T.FUJII

OFFPRINT/SONDERDRUCK/TIRE-A-PART

Tokyo / Japan / 1995

# Three-dimensional tomographic visualization of natural fracture networks and graph theory analysis of the transport properties

## Visualisation tomographique tridimensionnelle des réseaux de fractures naturelles et analyse de la théorie graphique des propriétés de transport

## Dreidimensionale tomographische Visualisierung von natürlichen Bruchvernetzungen und eine Graphiktheorie-Analyse der Transporteigenschaften

LAURA J. PYRAK-NOLTE & CARLO D. MONTEMAGNO, Department of Civil Engineering and Geological Sciences, University of Notre Dame, Ind., USA
GEMEI YANG & NEVILLE G.W. COOK, Department of Materials Science and Mineral Engineering, University of California, Berkeley, Calif., USA
LARRY R. MYER, Earth Sciences Division, Lawrence Berkeley Laboratory, Calif., USA

ABSTRACT: We analyze the spatial persistence of fracture network porosity and mean network aperture over the length of core samples containing natural fracture networks. By combining medical imaging algorithms with a Wood's metal injection technique, the three-dimensional geometry of fracture networks subjected to reservoir conditions is visualized and analyzed. The transport properties of the reconstructed fracture network geometry is analyzed using graph theory to examine the capillary pressure-saturation relationship for the network.

RESUME: Les resultats d'une etude complete en laboratoire du tridimensionnel geometrie de la reseau de fractures sont resumé et analyses. Une technique d'injection de métal est utilise avec une technique de Medical Imaging, elle fournit des résultats quantitatifs sur l'exacte géometrie des reseau de fractures.

ZUSAMMENFASSUNG: Wir analysieren die raumliche Beständigkeit der Porosität einigem Kluftnetz in Steinkohle, und auch die durchschnittliche Öffnung diesen Kluftnetz. Diese Drei-Dimensionalen Eigenschaften sind erzielen durch ein Metaleinspritz-verfahren, susammen mit Medizinische Abblidung. Hydraulische Eigenschaften dem Kluftnetz sind computiert durch Graph Theorie.

## 1 INTRODUCTION

Fracture network geometry influences the stability of rock masses and controls the movement of fluids through the rock mass. Fracture networks in rocks are often observed in only two-dimensional cross-sections such as at rock outcroppings, tunnel walls, and boreholes. Observing the three-dimensional network geometry is difficult especially with depth. At issue is whether or not the observed two-dimensional topology can be extended into the rock mass or with depth into the earth. Because of lithostatic stresses and local stress regimes, the spatial persistence of fracture network geometry would be expected to be affected with depth because fractures that are open at the surface may be closed or may not exist at depth. The difficulty has been in quantifying the spatial persistence in network geometry and such basic properties as network porosity. Remote techniques such as cross-hole seismic tomography may indicate that a fracture network still exists at depth but cannot indicate interconnectivity or whether it will support flow. The cross-hole tomographic results are often correlated with surface expressions of fracture networks to predict subsurface behavior.

In this paper, we analyze the spatial persistence of fracture network porosity and mean network aperture over the length of core samples containing natural fracture networks. By combining medical imaging algorithms with a Wood's metal injection technique, the three-dimensional geometry of fracture networks subjected to reservoir conditions is visualized and analyzed. The transport properties of the reconstructed fracture network geometry is analyzed using graph theory to examine the capillary pressure-saturation relationship for the network.

## 2 Experimental Procedure

### *2.1 Samples*

Four samples were used to investigate the geometrical properties of natural fracture networks (cleats) in coal. Samples IC2 and BC7A are whole drill core from the Intermediate and Basal Fruitland Formation, respectively, from the Valencia Canyon So. Ute #32-1 well, San Juan Basin, La Plata County, Colorado. Samples AA and BB were cored from blocks of coal from Seam #1 in the Sundance Pit at the La Plata coal mine, San Juan County, New Mexico. Core AA was taken perpendicular to the bedding planes. Core BB was cored parallel to the bedding planes and parallel to the dominant fracture set (face cleat). Sample dimensions are given in Table 1.

Table 1. Dimensions and Data from Wood's Metal Injection Experiments on Coal Samples IC2, BC7A, AA, and BB.

| Sample Number | IC2 | BC7A | AA | BB |
|---|---|---|---|---|
| Sample Dimensions: | | | | |
| Diameter (cm) | 9.2 | 9.2 | 8.9 | 8.9 |
| Length (cm) | 10.2 | 9.3 | 4.4 | 11.2 |
| Volume ($cm^3$) | 670 | 624 | 274 | 694 |
| Effective Pressure at Solidification (MPa) | 6.52 | 7.44 | 4.4 | 5.1 |
| Minimum Aperture Penetrated[1] (μm) | 1.78 ± 0.06 | 1.66 ± 0.06 | 2.44 ± 1.18 | 2.74 ± 1.30 |
| Weight of Injected Wood's Metal (grams) | 6.77 | 7.562 | 2.14 | 6.19 |
| Volume of Connected Voids[2] ($cm^3$) | 0.70 ± 0.019 | 0.759 ± 0.024 | 0.22 ± 0.005 | 0.65 ± 0.013 |
| Effective Cleat Porosity from Wood's Metal Injection[2] (%) | 0.104 ± 0.0028 | 0.121 ± 0.0039 | 0.082 ± 0.002 | 0.094 ± 0.002 |
| Effective Pressure during Helium-Water Drive (MPa) | 5.7 | 6.86 | 2.2 | 6.65 |
| Effective Cleat Porosity from Helium-Water Drive (%) | 0.30 | 0.45 | 0.22 | 0.11 |

[1] *Error from deviations in surface tension and contact angle of Wood's Metal*
[2] *Error from deviations in the density of Wood's metal*

### 2.2 *Experimental Set-up*

The porosity of the fracture network was measured using a Wood's metal injection method and a water-helium drive method. In the water-helium drive method, the coal core is saturated with a brine and subsequently displaced with humidified helium. The volume of brine produced is recorded and used to establish the porosity of the sample (Gash 1991; Gash 1992). Wood's metal injection was first used by Dullien (1969, 1981) to capture the geometry of pores in sandstone. It has been subsequently used to examine the void geometry of single natural fractures, the growth of cracks under compressive stress, and the distribution of two-phases in pores of sandstone (Yadav 1984; Pyrak-Nolte 1987; Zheng 1989). The physical properties of Wood's metal are listed in Table 2. The Wood's metal injection technique is similar to mercury porosimetry where the size of aperture penetrated is proportional to the injection pressure. The advantage of using a Wood's metal method over mercury porosimetry is that the metal leaves a detailed cast of the void space. The advantage of the Wood's metal method over traditional resin techniques is that the size of the aperture (void) penetrated can be controlled.

The Wood's metal injection method begins by placing the coal sample in a hydrostatic pressure vessel where it is subjected to effective pressures (Table 1) representative of reservoir conditions. The vessel is heated to approximately 95 $^{o}$C. A nitrogen back pressure is used during heating to prevent oxidation of the coal (Nelson 1989) and to provide a constant pressure front to the invading metal. Molten Wood's metal is injected into the sample and allowed to solidify. After injection, X-ray computerized tomography is used to delineate the metal-filled fractures within the coal cores. From the two-dimensional scans, the three-dimensional fracture network geometry is reconstructed.

Table 2. Properties of Wood's Metal (Cerrosafe®)

| | |
|---|---|
| Components: | |
| Bismuth | 42.5 % |
| Lead | 37.7 % |
| Tin | 11.3 % |
| Cadmium | 8.5 % |
| Melting Temperature Range ($^{o}$C) | 70 $^{o}$C - 88 $^{o}$C |
| Surface Tension (dynes/cm) | 485 $\pm$ 17 |
| Contact Angle on Coal | 130$^{o}$ $\pm$ 21$^{o}$ |
| Density (grams/cm$^3$) | 9.83 $\pm$ 0.29 |
| Young's Modulus (GPa) | 9.7 |

## 3 EXPERIMENTAL RESULTS

Combining Wood's metal injection with x-ray tomography yields information on the aperture distribution of the fracture network, the porosity of the fracture network, and the geometrical properties of the fracture network (e.g. length, orientation, spatial correlations). The porosity of the fracture network for each sample, based on the Wood's metal injection experiments, is given in Table 1 along with the porosity determined from the helium-water drive technique.

The porosity from the Wood's metal method is determined by dividing the volume of injected metal by the bulk volume of the sample. This effective fracture network porosity is for apertures greater than the minimum aperture penetrated by the Wood's metal which ranged between 2 to 3 microns for all of the samples (Table 1). The minimum aperture penetrated is calculated from Laplace's equation for capillary pressure in a cylindrical tube using the pore pressure at solidification, the contact angle of Wood's metal on coal, and the surface tension of Wood's metal. The effective network porosity determined with the Wood's metal method is less than that determined by the water helium-drive. Because of the high surface tension of Wood's metal, the size of the pores accessed by the metal is limited to the large apertures compared to pores that can be accessed by helium.

## 4 IMAGE ANALYSIS

Through image analysis of the x-ray tomographic scans (CT scans), the aperture distribution of the fracture network, the variation of porosity with depth in the sample, and spatial correlations of apertures can be determined (Pyrak-Nolte & Montemagno, 1994; Montemagno & Pyrak-Nolte, 1995a&b). Because the x-ray sources of CT scanners typically do not produce a monochromatic beam of photons, selective attenuation of photons of different energies results in the generation of beam hardening artifacts that exaggerate the thickness (aperture) of the Wood's metal-filled fractures and reduces the achievable resolution of the two-dimensional CT scans from 0.3 mm to greater than 1 mm. Visual examination of the Wood's metal-filled fractures established that the fracture apertures were typically less than 0.1 mm and ranged between 30 μm - 90 μm, which is much less than the optimal resolution of the CT scanner. The resolution of the CT images is a 0.3 mm by 0.3 mm pixel can. Because the fracture apertures were smaller than the dimensions of one pixel, the imaged fracture apertures were reduced to a width of one pixel within each two-dimensional scan. The position of the fracture aperture was established to an accuracy of 0.3 mm (Figure 1).

Figure 1 shows the geometry of the fracture network for the four coal samples at different depths within each core. Images of the fracture network for Core AA and BB show the anisotropy of the fracture network geometry in coal because these cores were drilled orthogonal to each other. Compared to Core IC2, Core BC7A contained more fractures though it was obtained from a deeper depth. However, this observation correlates with well-test data that found that the Basal Fruitland formation (~ 580 m) had a higher permeability than the Intermediate Fruitland formation (~540 m).

The porosities of the fracture networks in the coal cores were determined by determining the aperture of the fractures from the CT density and spatial location information. The logarithm of the magnitude of absorption (or CT number, CT#) of an x-ray beam is linearly proportional to the thickness of the absorbing material. The constant of proportionality, F, relates the CT number to the volume density of metal within the voxel (Montemagno & Pyrak-Nolte, 1995b).

$$\sum_{N} Voxel\ Volume * CT_N * F = \frac{Reconstructed\ Volume}{Bulk\ Volume} * Volume\ of\ Metal\ Injected \qquad (4.1)$$

Multiplying the volume density of metal within a voxel by the area of the pixel face of the voxel gives the aperture of the fracture at that voxel location. The minimum and maximum aperture resolved through image analysis depends on a threshholding procedure of the image which eliminates the non-fracture portions of the sample, that is the coal, shale fingers, bedding planes, etc. The range of CT numbers that represent the fracture are constrained by the injected metal volume. Table 3 gives the minimum and maximum aperture for each coal core. From Table 3, the minimum aperture is about an order of magnitude larger than the minimum aperture penetrated by the metal. A CT number threshold of 1400 was used for Cores AA and BB, and a threshold of 1900 was used for cores IC2 and BC7A.

Table 3. Minimum and maximum aperture resolve through image analysis and constraint of Wood's metal injection data.

| Core Number | Minimum Aperture (microns) | Maximum Aperture (microns) |
|---|---|---|
| AA | 34 | 51 |
| BB | 38 | 105 |
| IC2 | 39 | 93 |
| BC7A | 58 | 116 |

Figure 2(a-d) shows the variation in porosity and mean aperture with depth in the sample for the four coal cores. Ten millimeters from the inlet and outlet side of the cores has been removed to exclude end effects from the Wood's metal injection except for core AA on the inlet side. For all of cores, the porosity is not constant throughout the core. A one-dimensional auto-correlation analysis was performed to determine the spatial persistence of the porosity. This measure represents a qualitative indication of the length scale over which the interconnectivity and/or void geometry is maintained. Table 4 contains the correlation length for the four coal cores. No correlation of porosity with depth in the sample was observed for Core AA. The correlation length for cores IC2 and BC7A are on the order of several millimeters. Based on this analysis, porosity of a fracture network under to in-situ conditions can only be projected a few millimeters into a core sample.

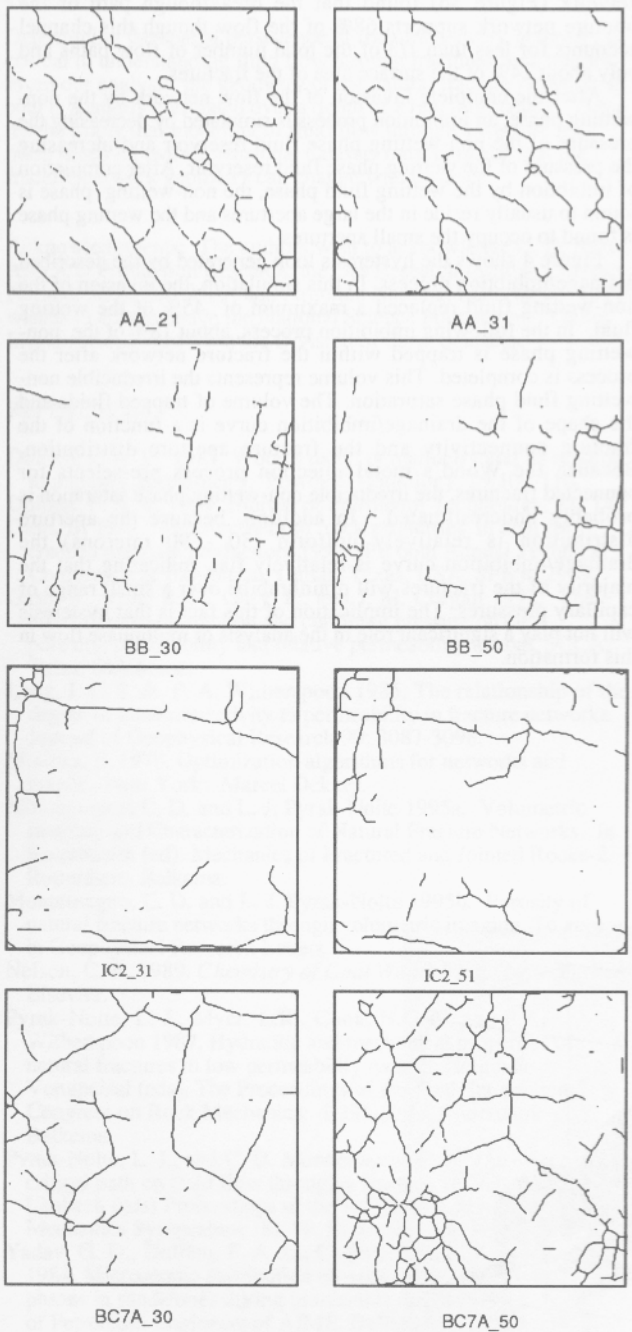


Figure 1. Two-dimensional images (60 mm by 60 mm)) of fracture network for different depths within the coal cores from CT scans that were processed to remove beam hardening effects. The sample name is followed by the depth of the slice in mm.

For all of the cores the variation in porosity with depth shows no correlation with the variation in mean aperture with depth. If the number of fractures in the network were constant, the porosity and mean aperture would have a linear correlation, that is an increase in porosity would be accompanied by an increase in mean aperture. The change in number of fractures with depth in a sample is observed from the reconstructed two-dimensional images of the fracture network.

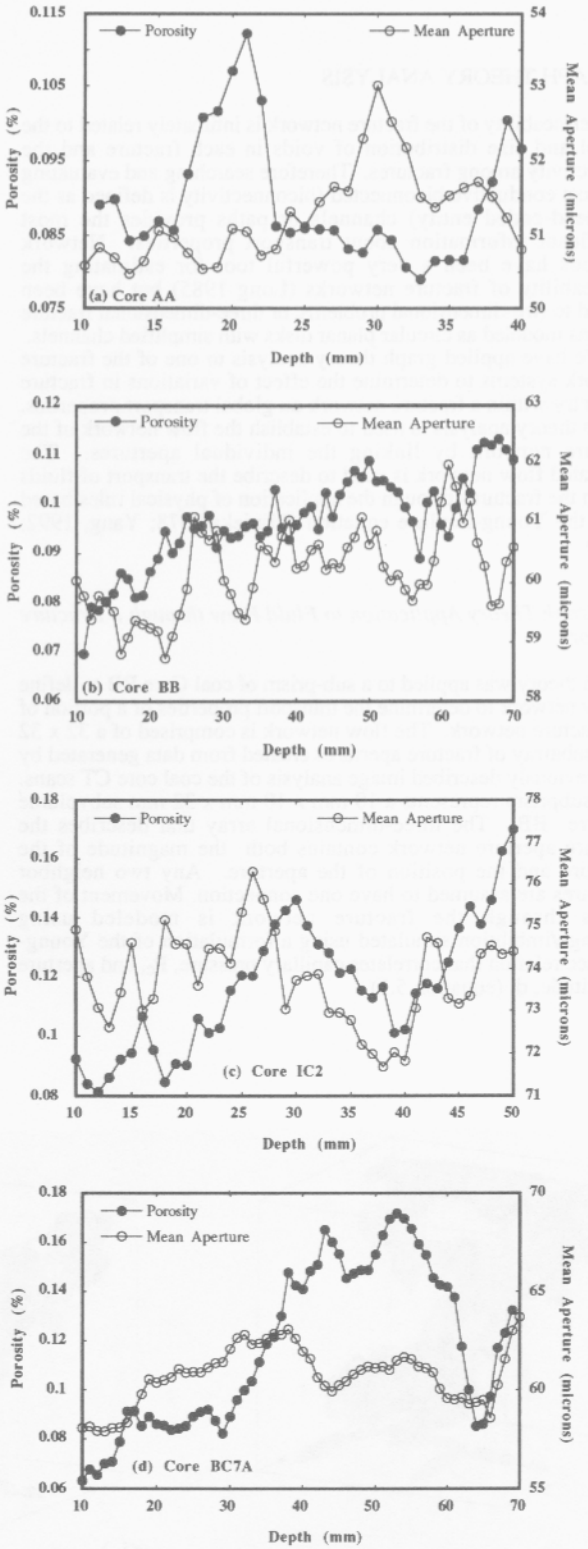


Figure 2. The variation in the porosity and mean aperture of the fracture network with depth in the sample for coal cores (a) AA, (b) BB, (c) IC2, and (d) BC7A.

Table 4. Correlation length of fracture network porosity.

| Core Number | Correlation Length (mm) |
|---|---|
| AA | 0 |
| BB | 16 |
| IC2 | 4 |
| BC7A | 5 |

## 5 GRAPH THEORY ANALYSIS

The permeability of the fracture network is intimately related to the spatial and size distribution of voids in each fracture and the connectivity among fractures. Therefore searching and evaluating the most conductive biconnected (biconnectivity is defined as the non-dead-ended entity) channels or paths provides the most significant information about transport properties. Network methods have been a very powerful tool for estimating the permeability of fracture networks (Long 1985) but have been limited to two-dimensional problems, or three-dimensional fracture systems modeled as circular planar disks with simplified channels.

We have applied graph theory analysis to one of the fracture network systems to determine the effect of variations in fracture geometry within a fracture network on global transport properties. Graph theory analysis is used to establish the flow network of the fracture network by linking the individual apertures. The generated flow network is used to describe the transport of fluids within the fractures through the application of physical rules based upon the Young-Laplace equation (Minieka,1978; Yang, 1992; 1993).

### *5.1 Graph Theory Application to Fluid Flow through a Fracture Network*

Graph theory was applied to a sub-prism of coal Core BB to define a flow network to determine the transport properties of a portion of the fracture network. The flow network is comprised of a 32 x 32 x 32 subarray of fracture apertures created from data generated by the previously described image analysis of the coal core CT scans. This subprism represents a 10 mm x 10 mm x 32 mm subvolume of core BB. The three-dimensional array that describes the fracture aperture network contains both the magnitude of the aperture and the position of the aperture. Any two neighbor apertures are assumed to have one connection. Movement of the fluids through the fracture network is modeled using drainage/imbibtion simulated using a formulation of the Young-Laplace relation that correlates capillary pressure, $P_c$, and aperture magnitude, d, (equation 5.1).

$$P_c = \frac{4\sigma\cos\theta}{d} \qquad (5.1)$$

Simulation of the drainage/imbibition process is performed by first establishing constant pressure boundaries on the opposing inlet and outlet faces of the subprism. No flow boundaries are established on the other four side walls of the computational domain. The inlet face of the domain is assumed to be connected to an infinite non-wetting fluid phase reservoir, and likewise the outlet side of the fracture network is connected to an infinite wetting fluid phase reservoir. Initially the fractures are assumed to be filled with wetting phase fluid. The pressure of the non-wetting phase fluid reservoir is increased to initiate its invasion into the fracture network. Figure 3a shows the connectivity of the fracture network at the moment the non-wetting fluid phase breaks through into the wetting fluid phase reservoir. The invading fluid path is through the path of largest apertures. Analysis of the fully invaded network (Figure 3b) found that the breakthough path of the fracture network supports 68% of the flow though this channel accounts for less than 1/3 of the total number of flow paths and only about 24% of the surface area of the fractures.

After the complete invasion of the flow network by the non-wetting phase, an imbibition process is simulated by decreasing the pressure of the non-wetting phase fluid reservoir and increasing the pressure of the wetting phase fluid reservoir. After completion of imbibtion by the wetting fluid phase, the non-wetting phase is found to usually reside in the large apertures and the wetting phase is found to occupy the small apertures.

Figure 4 shows the hysteresis loop generated by the described drainage/imbibtion process. In this simulation, the invasion of the non-wetting fluid replaced a maximum of 45% of the wetting fluid. In the following imbibition process, about 18% of the non-wetting phase is trapped within the fracture network after the process is completed. This volume represents the irreducible non-wetting fluid phase saturation. The volume of trapped fluids and the shape of the drainage/imbibition curve is a function of the fracture connectivity and the fracture aperture distribution. Because the Wood's metal injection process pre-selects for connected fractures, the irreducible non-wetting phase saturation is probably underestimated. In addition, because the aperture distribution is relatively uniform (30 - 90 microns) the drainage/imbibition curve is relatively flat, indicating that the majority of the fractures will drain/imbibe over a small range of capillary pressures. The implication of this fact is that hysteresis will not play a significant role in the analysis of multiphase flow in this formation.

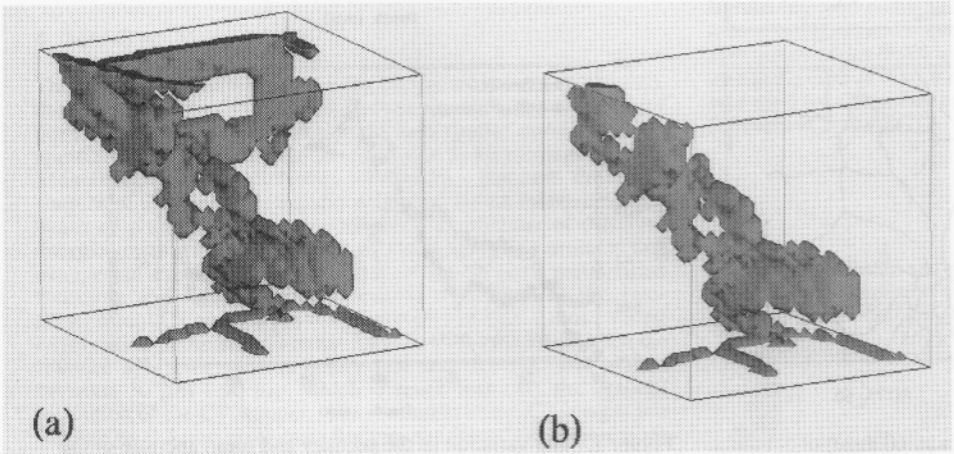


Figure 3. Three-dimensional visualization of the non-wetting phase flows in a subvolume of the natural fracture network in Core BB. (a) Fully invaded; (b) At breakthrough.

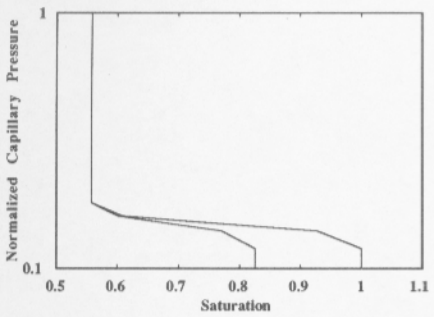


Figure 4. Simulated drainage/imbibition curve for a sub-volume of the fracture network in Core BB.

## 6 SUMMARY

Determining the spatial persistence of fracture network geometry is critical to understanding fluid flow through fractured rock masses. From our analysis, the geometry of the natural fracture networks in coal is spatially correlated over a depth of a few millimeters. These results imply that modeling of fluid flow through a fracture rock mass based on two-dimensional datasets must consider that the fracture network geometry can change with distance.

Acknowledgments: The authors wish to acknowledge D. D. Nolte, AMOCO Production Research, the Gas Research Institute Contract Number 5092-260-2507, and Argonne National Laboratory. LJPN wishes to acknowledge the National Science Foundation - Young Investigator Award from the Division of Earth Sciences.

## REFERENCES

Dullien, F. A. L. 1981. Wood's metal porosimetry and its relation to mercury porosimetry. Powder Technology. 29:109-116.

Dullien, F. A. L. 1969. Journal of Petroleum Technology. 21: 14.

Gash, B. 1991. Measurement of 'rock properties' in coal for coalbed methane production. 1991 SPE 66th Annual Technical Conference & Exhibition, Dallas, Texas, USA, SPE #22909.

Gash, B., Volz, R. F., Gary, P., and J. M. Corgan 1992. The effect of cleat orientation and confining pressure on cleat porosity, permeability and relative permeability in coal. SCCA, Tulsa, Oklahoma,

Long, J. C. S. & P. A. Witherspoon 1985. The relationship of the degree of interconnectivity to permeability in fracture networks. Journal of Geophysical Research 90: 3087-3098.

Minieka, E. 1978. Optimization algorithms for networks and graphs. New York: Marcel Dekker.

Montemagno, C. D. and L. J. Pyrak-Nolte 1995a. Volumetric Imaging and Characterization of Natural Fracture Networks. In Rossmanith (ed). Mechanics of Fractured and Jointed Rocks-2. Rotterdam: Balkema.

Montemagno, C. D. and L. J. Pyrak-Nolte 1995b. Porosity of natural fracture networks through volumetric imaging. To appear in Geophysical Research Letters.

Nelson, C. R. 1989. *Chemistry of Coal Weathering*. New York: Elsevier.

Pyrak-Nolte, L. J., Myer, L.R., Cook, N.G.W. and P.A. Witherspoon 1987. Hydraulic and mechanical properties of natural fractures in low permeability rock. In Herget & Vongpaisal (eds), The Proceedings of the Sixth International Congress on Rock Mechanics: 1:225-233. Rotterdam: Balkema.

Pyrak-Nolte, L. J., and C. D. Montemagno 1994. The effect of the critical path on fluid flow through a fracture. In Nelson & Laubach (eds) Proceedings of the 1st North American Rock Mechanics Symposium: 81-88. Rotterdam: Balkema.

Yadav, G. D., Dullien, F. A .L., Chatzis, I. and I.F. MacDonald 1984. Microscopic distribution of wetting and non-wetting phases in sandstones during immiscible displacements. Society of Petroleum Engineers of AIME. Dallas, Texas. SPE 13212.

Yang, G. 1992. *Computer Aided Analysis of Groundwater and Polluntant Migration Caused by Strata Movement*. Ph.D. Thesis. University of California, Berkeley.

Yang, G., N. G. W. Cook, and L. R. Myer 1993. Analysis of preferential flow paths using graph theory. In Proceedings of the 34th U.S. Rock Mechanics Symposium: 1423-1430.

Zheng, Z. 1989. *Compressive Stress-Induced Microcracks in Rocks and Applications to Seismic Anisotropy and Borehole Stability*. Ph.D. Thesis. University of California, Berkeley.